Particle size control of cathode components for high-performance all-solid-state lithium-sulfur batteries

Bo Fan, Zebo Guan, Lilin Wu, Shibang Zhang, Manlin Tan, Zhongkuan Luo, Xianghua Zhang, Hongli Ma, Bai Xue

Particle size control of cathode components for high-performance all-solid-state lithium-sulfur batteries

Bo Fan[a], Zebo Guan[a], Lilin Wu[b,c], Shibang Zhang[a], Manlin Tan[d], Zhongkuan Luo[b], Xianghua Zhang[c], Hongli Ma[c], Bai Xue[a,*]

a Shenzhen Key Laboratory of Advanced Thin Films and Applications, College of Physics and Optoelectronic Engineering, Shenzhen University, 518060 Shenzhen, China

b College of Chemistry and Environmental Engineering, Shenzhen University, 518060 Shenzhen, China

c Laboratory of Glasses and Ceramics, Institute of Chemical Science, University of Rennes 1, Rennes 35042, France

d Research Institute of Tsinghua University in Shenzhen, Shenzhen 518055, China

* Corresponding author, Tel: +86 (0)755 26534995, E-mail address: baixue@szu.edu.cn

Abstract

Understanding the size effect of each component on battery performance is essential for designing high-performance Li_2S/S cathode for all-solid-state Li-S batteries (ASSLSBs). However, the size effects of different components are always coupled because ball-milling, an indispensable process to synthesize reversible cathode, simultaneously and uncontrollably reduces the particle size of all the components. Here, a liquid-phase method, without ball-milling, is developed to synthesize the Li_2S composite cathode, so that the particle size of the active material Li_2S and the solid electrolyte Li_3PS_4 (LPS) can be independently controlled at nanoscale or at microscale. This helps reveal that compositing Li_2S and the conductive agent at nanoscale is essential for enhancing the reaction kinetics, while the nanoscale particle size and homogenous distribution of LPS is important for accommodating the large volume change of

This article has been accepted for publication and undergone full peer review but has not been through the copyediting, typesetting, pagination and proofreading process, which may lead to differences between this version and the Version of Record. Please cite this article as doi: 10.1111/jace.19220.

the cathode. By reducing the particle size of Li_2S to 9.4 nm and that of LPS to 44 nm, the liquid-phase-synthesized composite cathode exhibits reversible capacity and 100% utilization of Li_2S under 0.1 C rate.

Keywords: all-solid-state battery; glass-ceramics; ionic conductivity; particle size; sulfides

1.Introduction

Lithium-sulfur batteries with high theoretical specific capacity (1672 mAh g^{-1} to S) and energy density (2600 W h kg^{-1}) are considered as one of the best candidates for next-generation energy storage system. [1, 2] However, traditional lithium-sulfur batteries with liquid organic electrolyte suffer from many issues, such as polysulfide shuttling, lithium-dendrite growth, poor thermal stability and flammability which lead to capacity fading and safety issues [3]. In order to address these problems, researchers turned their attention to all-solid-state lithium-sulfur batteries (ASSLSBs). Benefitting from inorganic solid electrolyte, not only the polysulfide shuttling is suppressed, but also the safety problems are eliminated [2]. However, the development of ASSLSBs is limited by many difficulties, such as the poor contact of solid-solid interfaces, slow reaction kinetics, large volume expansion of the cathodes and low utilization of the active materials [4]. Lithium sulfide (Li_2S), whose theoretical capacity is 1166 mAh g^{-1} to Li_2S, is a widely used cathode material for lithium-sulfur batteries [1, 5]. By using Li_2S as the active material, lithium-free anode batteries can be prepared [6, 7], thus improving the product safety. However, as same as sulfur, the ionic/electronic conductivity of Li_2S is very low, resulting in high polarization and low utilization of the active material [8].

So far, many strategies have been attempted to improve the ionic/electronic conductivity and to alleviate the influence of stress/strain of Li_2S-based cathode [9-14]. A basic idea behind these strategies is that reducing the particle size of the components in the composite cathode and mixing them at nanoscale can both reduce the diffusion path of the ions and electrons, and improve the structural stability of the cathode against the volume change. For example, El-Shinawi et al. reported a microwave approach to synthesis nanostructured Li_2S cathode showing a stable cycling performance and capacity (400 cycles and 440 mAh g^{-1} under 0.5 C at 60℃) [15]. Yan et al. prepared composite cathodes with carbon-wrapped Li_2S nanoparticles (<50 nm), by combustion of lithium metal with CS_2, and it could effectively increase the utilization of Li_2S, thus improving the battery performance [14]. Jiang et al. obtained nanostructured Li_2S particles (~15 nm) deposited on CNTs by a liquid-phase method. The battery shows a steady cycling performance of 300 cycles under 1.0 C at 60℃ [16].

Although the idea of "reducing particle size" consciously or unconsciously guides the development of the composite cathode of the ASSLSBs, it is unclear whether the particle size of the active material and the solid electrolyte play different roles on the battery performance, and what is the critical particle size required to achieve fast reaction kinetics. The answers to these questions are rewarding for designing more rational structure of the composite cathode of the ASSLSBs. A major challenge of this study is that, in most studies, ball-milling is an indispensable process to synthesize the composite cathode, which simultaneously and uncontrollably reduces the particle size of all the components in the cathode, making it impossible to study the size effect of each component independently.

In this work, a liquid-phase method, without a ball-milling process, is developed to synthesize the Li_2S composite cathodes. With this method, the particle size of the active material Li_2S and the solid electrolyte Li_3PS_4 (LPS) can be independently controlled at nanoscale or at microscale. The different combination of the particle size obtains three cathodes, the nano-Li_2S – nano-LPS cathode, the nano-Li_2S – micro-LPS cathode and the micro-Li_2S – nano-LPS cathode. By comparing their electrochemical properties, the size effects of the active material and the solid electrolyte on the battery performance can be decoupled. A conclusion is drawn that compositing Li_2S and the conductive agent at nanoscale is essential for enhancing the reaction kinetics, while the nanoscale particle size and homogenous distribution of LPS is important for accommodating the large volume change of the cathode. Moreover, a modified galvanostatic intermittent titration technique (GITT) for phase-transformation electrode is conducted [17]. This quantitatively provides the critical size of Li_2S to ensure the reaction kinetics.

Experimental

Materials and synthesis

The starting materials were Li_2S (99.9%, Alfa Aesar), P_2S_5 (99%, Qingdao Yurui Ltd.), sublimated sulfur (99.5%, Alfa Aesar), $LiEt_3BH$ (dissolved in tetrahydrofuran, 1 M, Innochem), Ketjen Black (KB, ECP600JD), anhydrous tetrahydrofuran (THF, ⩾99.9%, Aladdin) and anhydrous acetonitrile (ACN, 99.8%, Aladdin). All the chemicals were used as is, without further purification.

Synthesis of $80Li_2S{\cdot}20P_2S_5$ solid electrolyte

$80Li_2S{\cdot}20P_2S_5$ glass-ceramic electrolyte was synthesized as described in our previous study [18]. Briefly, A mixture of Li_2S and P_2S_5 with molar ratio of 80:20 was ball milled for 70 h at 450 rpm, using a planetary ball mill apparatus (Pulverisette 7, Fritsch GmbH, Germany). The ball milling was conducted in an argon-filled glovebox (O_2 < 0.5 ppm, H_2O < 0.5 ppm). After then, the resultant glassy powder was sealed in a silica glass tube under vacuum and heat-treated at 260℃ for 1 h to obtain the $80Li_2S{\cdot}20P_2S_5$ glass-ceramic powder. The $80Li_2S{\cdot}20P_2S_5$ glass-ceramic exhibits good compatibility with lithium anode [19]. Moreover, its ionic conductivity is much higher than that of the liquid-phase synthesized LPS (Figure S1, 1.65 mS cm^{-1} for $80Li_2S{\cdot}20P_2S_5$ glass-ceramic and 0.29 mS cm^{-1} for liquid-phase synthesized LPS at 60 °C). Therefore, $80Li_2S{\cdot}20P_2S_5$ glass-ceramic was used to prepare the separator between the cathode and the anode.

Synthesis of nano-LPS and micro-LPS

Li_3PS_4 nanoparticles, denoted as nano-LPS, were synthesized by a dual precursor method developed in our laboratory recently [20, 21]. Firstly, the sulfur powder and the THF solution containing $LiEt_3BH$ (1 M) were stoichiometrically mixed and stirred. With the reaction $S+2LiEt_3BH = Li_2S+H_2+2Et_3B$, a Li_2S sol was obtained. After purified by centrifugation, the Li_2S sol was redispersed in THF with a concentration of 0.16 M. Then, a mixture of commercial Li_2S and P_2S_5 with a molar ratio of 1:1 was stirred in ACN for 30 min to obtain $Li_2S{\cdot}P_2S_5$ solution with a concentration of 0.13 M. Finally, the two precursors, Li_2S sol and $Li_2S{\cdot}P_2S_5$ solution, were mixed and stirred to obtain a sol containing nano-LPS, by the reaction $2Li_2S+Li_2S{\cdot}P_2S_5 = 2Li_3PS_4$. The nanoparticles in the sol have a particle size of 44 nm (Figure S2). The solvent could be

completely removed after drying at 60 °C and further heat-treatment at 250 ℃ under vacuum for 1 h. The ionic conductivity turned out to be 0.29 mS cm^{-1} at 60 °C.

The micro-sized Li_3PS_4 particles, denoted as micro-LPS, were prepared using the conventional suspension synthesis route [22]. Briefly. 0.16 g of a mixture of commercial Li_2S and P_2S_5 with moral ratio of 3:1 was stirred in 16 ml of ACN for 48 h to obtain the white suspension containing micro-LPS. After removing the solvent, the ionic conductivity of the micro-LPS turned out to be 0.16 mS cm^{-1} at 60 °C.

Synthesis of the cathode composites

Three Li_2S composite cathode were synthesized for comparison.

For the first cathode, KB was firstly stirred in the THF solution containing $LiEt_3BH$ (0.5 M) for 24 h. Then sulfur powder was added to the resultant suspension and stirred for several minutes, so that nano-Li_2S particles generated on the KB. This nano-Li_2S @ KB composite was purified by centrifugation and re-dispersed in THF. Then the sol containing nano-LPS was added to the suspension of nano-Li_2S @ KB and stirred for 30 min to mix thoroughly. Finally, the precursor was dried at 60 °C and further heat-treated at 250 ℃ under vacuum for 1 h to obtain the composite cathode. The weight ratio of Li_2S, LPS and KB is 12:60:28. This cathode is denoted as nano-Li_2S – nano-LPS.

For the second cathode, the suspension containing nano-Li_2S @ KB was firstly prepared. Then the suspension containing micro-LPS was added to this suspension and stirred for 30 min to mix thoroughly. Finally, the precursor was dried at 60 °C and further heat-treated at 250 °C

under vacuum for 1 h. The weight ratio of Li_2S, LPS and KB is 12:60:28. The obtained cathode is denoted as nano-Li_2S – micro-LPS.

For the third cathode, a mixture of commercial Li_2S and KB was stirred in THF for 24 h. Then, the sol containing nano-LPS was added to this suspension and stirred for 30 min. After drying at 60 °C and further heat-treatment at 250 °C under vacuum for 1 h, the composite cathode, denoted as micro-Li_2S – nano-LPS, was obtained.

Characterization of materials

The phase structure was tested by an X-ray diffractometer (XRD, D8-Advanced, Bruker AXS GmbH, Germany) using Cu-K_α radiation (λ=1.504 Å). To avoid the moisture, the samples were mounted in a sample holder and sealed by polyimide cover films in the glovebox prior to the XRD characterization. The morphological and elemental analysis were conducted by a field-emission scanning electron microscope (SEM, Zeiss Supra 55, Carl Zeiss GmbH, Germany) equipped with an energy dispersive X-ray spectroscopy accessory (EDX). Samples were transferred from the glovebox to SEM through a vacuum sample holder. Transmission electron microscopy (TEM) images, high-angle annular dark-field (HAADF) image and electron energy loss spectra (EELS) were recorded by a double Cs-corrected transmission electron microscope (Titan Cubed Themis G2 300). The specific surface area was measured with the Brunauer–Emmett–Teller (BET, BELSORP MAX, Microtrac MRB, Japan) method.

Electrochemical performance testing

ASSLSBs were assembled as follow. Firstly, 280 mg $80Li_2S{\cdot}20P_2S_5$ glass-ceramic powder was cold-pressed into pellet (15 mm diameter and ~ 1 mm thickness) under a pressure of 80 MPa for 1 min. Then, 5 mg powder of composite cathode was spread on one side of the pellet and cold-pressed under a pressure of 330 MPa for 10 min, and a Li foil (11 mm diameter) was attached to the other side of the pellet. Finally, the pellet was packaged by a swagelok mold. All the batteries were assembled in an argon-filled glovebox (O_2 < 0.5 ppm, H_2O < 0.5 ppm).

The as-assembled ASSLSBs experienced an activating cycle with a constant current of 0.045 mA cm^{-2} (0.1 C rate) and a voltage range of 1.0-4.0 V [14], and then galvanostatic charge and discharge curves were recorded by a battery tester (LAND CTZ001A) with a voltage range of 1.0-3.6 V. The electrochemical impedance spectroscopy (EIS) measurements were performed at an electrochemical workstation (CHI660E, CH Instruments Ins., Shanghai, China). The frequency range was 10^{6}–10^{-2} Hz and the amplitude of AC signal was 5 mV. The impedance spectra were further fitted by using Zview software. The GITT was conducted to study the ion diffusion in the batteries. Each titration lasted for 15 min under 0.045 mA cm^{-2}, followed by a rest of 3 h. All the tests were conducted at 60℃. The lithium diffusion in the Li_2S nanoparticle was also simulated by a finite element method (FEM), using COMSOL Multiphysics. The detailed description of the model can be found in the Support Information.

Results and discussion

Characterization of the composite cathodes

Figure 1(a) shows the XRD patterns of the nano-Li_2S @ KB composite prepared by in-situ deposition of Li_2S on KB and the micro-Li_2S @ KB composite prepared by mixing commercial

Li_2S with KB. The diffraction peaks at 2θ = 26.7°, 31.12°, 44.63° and 53.04° for these two samples can be indexed to the diffraction from the (111), (200), (220) and (311) planes of crystalline Li_2S (JCPDS: 023-0396), and no impurities are observed. Moreover, the XRD of the nano-Li_2S @ KB shows significant peak broadening compared to the micro-Li_2S @ KB, illustrating that the particle size of the nano-Li_2S is much smaller than the commercial Li_2S. According to Debye-Scherrer formula, the particle size of nano-Li_2S is estimated to be 9.4 nm. Interestingly, the high-magnification SEM image of the nano-Li_2S @ KB in Figure 1(b) shows a porous structure similar to that of the pristine KB powders (Figure S3). We infer that the nano-Li_2S particles are deposited within the micropores of KB, forming the composite at nanoscale. This conclusion is further supported by the SEM EDS mapping (Figure 1(d)) and TEM EDS mapping (Figure S4) of the nano-Li_2S @ KB. It can be seen that the S element, which is representative for Li_2S, is homogenously distributed in the mapping and well overlaps that of C element, either at the micrometer-scale or at the hundred-nanometer-scale. Moreover, by using nitrogen adsorption/desorption isotherm analysis to measure the porosity of the nano-Li_2S @ KB, micro-Li_2S @ KB and pristine KB, as shown in Figure S5, it is found that the N_2-BET specific surface areas and pore volume of the nano-Li_2S @ KB (446 $m^2\ g^{-1}$ and 1.70 $cm^3\ g^{-1}$) are much smaller than those of the micro-Li_2S @ KB(1027 $m^2\ g^{-1}$ and 2.86 $cm^3\ g^{-1}$) and pristine KB (1976 $m^2\ g^{-1}$ and 5.03 $cm^3\ g^{-1}$), further confirming that the nano-Li_2S particles are deposited within the micropores of KB.

Differently, besides the porous structure of KB, micro-sized grains are observed in the SEM image of the micro-Li_2S @ KB in Figure 1(c). The SEM EDS mapping (Figure 1(e)) shows that besides the Li_2S nano-particles well mixed with KB, reflected by the background S distribution

over the sample, S-rich large particles with size of 10 - 20 μm are observed in the elemental mapping of the micro-Li_2S @KB composite, confirming the existence of micro-sized Li_2S particles in this sample.

Furthermore, the nano-Li_2S @ KB is characterized by TEM, as shown in Figure 2. The lattice spacing of the nano-crystallites in the high-resolution TEM image (HRTEM) is determined to be 0.28 and 0.33 nm (Figure 2(a)), corresponding to the (200) and (111) planes of Li_2S. From the HAADF image (Figure 2(b)), it can be seen that the nano-crystallites are brighter than the surrounding amorphous phase, which is coincident with that fact that S-rich region is brighter than C-rich region owing to the larger atomic number of S. Thus, the TEM directly detects that the Li_2S nano-crystallites are embed in KB. The observed particle size of the Li_2S nano-crystallites is ~ 10 nm, in good accordance with 9.4 nm that is determined from the XRD results by Debye-Scherrer formula.

The nano-Li_2S @ KB composite is mixed with nano-LPS and micro-LPS to form the nano-Li_2S – nano-LPS cathode and the nano-Li_2S – micro-LPS cathode, respectively. Meanwhile, the micro-Li_2S @ KB composite is mixed with nano-LPS to form the micro-Li_2S – nano-LPS cathode. Figure 3(a) shows the XRD patterns of the three composite cathodes. Besides the diffraction peaks belonging to Li_2S, additional peaks belonging to β-Li_3PS_4 and thio-LISICON II are observed. The XRD patterns of the nano-LPS and the micro-LPS are shown in Figure S6, confirming the signals of β-Li_3PS_4 and thio-LISICON II is from the liquid-phase synthesized LPS. It is worth noting that micro-LPS contains unreacted Li_2S and an impurity phase $Li_4P_2S_6$ which is converted from the unreacted $Li_2S{\cdot}P_2S_5$ [23]. Therefore, the sharp peaks belonging to

Li_2S in the XRD pattern of the nano-Li_2S – micro-LPS is introduced by the micro-LPS suspension. The XRD results demonstrate that the nano-Li_2S – nano-LPS cathode has smaller particle size than the other two cathodes. Furthermore, comparing the morphology of the nano-Li_2S – nano-LPS cathode (Figure 3(c)) with the nano-Li_2S @ KB composite (Figure 1(b)), it can be seen that the porous structure of the nano-Li_2S @ KB composite disappears after the addition of nano-LPS, indicating that the nano-LPS fills these pores. This makes the three components, nano-Li_2S, nano-LPS and KB, are well composited at nanoscale. Differently, both porous structure of the nano-Li_2S @ KB composite and the nanoflakes of micro-LPS can be identified in the nano-Li_2S – micro-LPS cathode (Figure 3(d)). Nanoflake is a typical morphology of LPS prepared by suspension method using ACN as the reaction medium [22]. Evidently, the micro-scale lateral size of the nanoflakes hinders the intimate contact with the nano-Li_2S @ KB composite. In addition, large particles of micro-Li_2S can be seen obviously in the SEM image of the micro-Li_2S – nano-LPS (Figure 3(e)). A schematic diagram is proposed in Figure 3(b) to illustrate the microstructure of the three cathodes. It is illustrated that the three components, Li_2S, LPS and KB, in the nano-Li_2S – nano-LPS cathode can contact with each other intimately, while the other two cathodes cannot form compact structure.

Battery performance

The ASSLSBs are assembled using the three composite cathodes and the cycling performance are shown in the Figure 4. By comparing the three ASSLSBs, the influence of the size of Li_2S and LPS particles on the battery performance can be independently evaluated.

Firstly, the influence of the particles size of the active material Li_2S is studied by comparing the two batteries with the nano-Li_2S – nano-LPS cathode and the micro-Li_2S – nano-LPS cathode. As shown by Figure 4(a), after one activating cycle, the nano-Li_2S – nano-LPS exhibits a discharge capacity of 1060 mAh g^{-1}. On the contrary, the initial discharge capacity of the micro-Li_2S – nano-LPS is only 277 mAh g^{-1}. In the next few cycles, the activation of Li_2S continues and the capacity increases slightly for both batteries [12-14, 24]. After then, the capacity of the nano-Li_2S – nano-LPS stabilizes and retains 1138 mAh g^{-1} after 30 cycles, indicating that the utilization of Li_2S approaches 100%, while that of the micro-Li_2S – nano-LPS gradually decreases to 204 mAh g^{-1}. The coulombic efficiency is slightly higher than 100% during the initial cycles, which is commonly observed in Li_2S-based ASSLSBs [10, 16], and is related with the gradual activation of the cathode materials [25]. As shown by the charge and discharge curves in Figure 4(b-c), the overpotential is 0.10 V at the 10^{th} cycle and 0.17 V at the 30^{th} cycle for the nano-Li_2S – nano-LPS, while it is 0.24 V at the 10^{th} cycle and 0.35 V at the 30^{th} cycle for the micro-Li_2S – nano-LPS, indicating the higher internal resistance of the latter composite cathode.

To identify the factors which contribute to the internal resistance, the EISs of the batteries at the 10^{th} and 30^{th} cycles are measured (Figure 5(a-b)). By fitting the EISs with the equivalent circuit (Figure 5(c)) proposed in our previous work [4], the internal resistance (Table S1 and S2) can be divided into three parts, as shown in Figure 5(d), the ohmic resistance R_1, the interfacial resistance R_2, and the charge transfer resistance R_3. The ohmic resistance is mainly associated with the ion transport in the solid electrolyte membrane as well as the ion/electron transport in the composite cathodes. The interfacial resistance R_2 is associated with the interphase layer

formed between the solid electrolyte and the active materials [26]. At the 10th cycle, R_1 and R_3 dominate the internal resistance in both samples. For the nano-Li_2S – nano-LPS and the micro-Li_2S – nano-LPS, R_1 is 51.8 Ω and 258.5 Ω respectively, and R_3 is 101.7 Ω and 375.5 Ω respectively. The larger R_1 in the micro-Li_2S – nano-LPS indicates a more sluggish ion/electron transport in the composite cathodes, and its larger R_3 indicates fewer active sites [26-30]. At the 30th cycle, much more evident increase of R_1, R_2 and R_3 is observed for the micro-Li_2S – nano-LPS than the nano-Li_2S – nano-LPS, which is ascribed to the more severe collapse of the ionic/electronic channels and deterioration of the contact between the channels and the active materials in the former, due to the large volume change of Li_2S/S during the cycling of the batteries. In summary, reducing the particle size of Li_2S and forming Li_2S and carbon composite at nanoscale is essential for achieving high capacity, low overpotential and good cycling stability of the ASSLSBs, which benefits from the creation of large amounts of active sites and the construction of stable ionic/electronic channels.

Secondly, the influence of the particles size of the solid electrolyte LPS is studied by comparing the two batteries with the nano-Li_2S – nano-LPS cathode and the nano-Li_2S – micro-LPS cathode. Unexpectedly, the nano-Li_2S – micro-LPS exhibits an initial capacity of 1112 mAh g^{-1} and a low overpotential of 0.10 V, approached those of the nano-Li_2S – nano-LPS. The capacity of the nano-Li_2S – micro-LPS even reaches a higher value of 1392 mAh g^{-1} after the complete activation of Li_2S, which may be attributed to the contribution of the unreacted Li_2S introduced by the micro-LPS. However, the capacity of the nano-Li_2S – micro-LPS dramatically decreases to 531 mAh g^{-1} after 30 cycles. The capacity retention is only 38.3%. Meanwhile, more evident increase of R_2 and R_3 is observed in comparison with the nano-Li_2S – nano-LPS (Figure

5(d)), indicating the more severe deterioration of the contact between the active materials and the ionic channels. From these results, it can be concluded that the particle size of the solid electrolyte has less influence on the initial performance of the ASSLSBs than that of the active material, but significantly affects the cycling stability.

Benefitting from the nanoscale size of both the active material and the solid electrolyte, the battery with the nano-Li_2S – nano-LPS cathode shows the best rate performance, exhibiting reversible discharge capacities of 1377, 886, 646 mAh g^{-1} at 0.045, 0.13, 0.22 mA cm^{-2} (Figure 4(d)). A stable operation of the battery over 100 cycles, at a current density of 0.13 mA cm^{-2} (0.3 C rate) is shown in Figure 4(e) and (f). It is demonstrated that the capacity is initially 987 mAh g^{-1} and keeps 786 mAh g^{-1} after 100 cycles, with a capacity retention of 79.63%. It also exhibits a stable overpotential of about 0.30 V. Moreover, the battery with the nano-Li_2S – nano-LPS cathode delivers the capacity of 473 mAh g^{-1} under 0.1 C rate at room temperature (Figure S7). It is emphasized that the composite cathodes of the ASSLSBs which can cycle stably are always prepared by ball-milling. Recently, Kanno et al. found that by directly mixing sulfur-carbon replica composites and micrometer-scale sulfide electrolyte particles in THF without ball milling, the battery capacity fades rapidly over several initial cycles [31]. Our work demonstrates that by simultaneously reducing the particle size of the active material and the solid electrolyte into nanoscale, the liquid-phase prepared Li_2S cathode can also cycle stably. Its performance is comparable with the counterparts prepared by ball-milling (Table S3).

GITT analysis

The GITT curves of the three Li_2S composite cathodes are shown in Figure 6(a). For all the three Li_2S composite cathodes, the equilibrium potential, which is depicted by the upper envelope of the GITT curve, stabilizes over the most part of discharge stage, and at the end of the discharge stage it drops suddenly. Remarkably, these features are different from those of $LiCoO_2$ cathodes, whose equilibrium potential continuously decreases over the whole discharge stage [32, 33]. If the electrode host material forms a single-phase solid solution with Li, like in $LiCoO_2$, it will exhibit a smooth sloping potential curve due to the gradual change of the composition. However, if the Li insertion resulting in a first-order phase transformation of the host materials, like in $LiFePO_4$, it will exhibit a potential plateau until the composition moves away from the two-phase region [34]. Therefore, the stable equilibrium potential of the Li2S composite cathode by GITT reveals that the cathode undergoes a first-order phase transformation. Kim et al. [35] studied the lithiation process of sulfur in carbon nanotubes by in-situ TEM, and observed the movement of a flat Li_2S/S phase boundary during the lithiation process, which confirming the direct conversion between S and Li_2S in carbon nanotubes. These TEM results imply that the first-order phase transformation of the Li_2S composite cathode in our ASSLSBs could be the direct conversion between S and Li_2S.

As shown by the schematic diagram in Figure S8, the discharge equilibrium potential curve can be divided into two regions, the two-phase region and the one-phase region. In the one-phase region, the relationship between the potential E and the composition of $Li_{\alpha+\delta}S$ can be established by the slope k of the potential curve, that is, $\mathrm{d}\delta/\mathrm{d}E = 2/kQ_{th}$. Here $Li_\alpha S$ ($\alpha \approx 2$) is the composition in equilibrium with S under strain-free condition, and Q_{th} is the theoretical capacity of Li_2S. In the two-phase region, gentle decrease of the potential can still be observed.

This could be attributed to the increasing strain accommodation energy owing to the volumetric expansion of the lithiated cathode [17]. This leads to the slight deviation of the composition from $Li_\delta S$ with $\delta = 2\Delta E/kQ_{th}$. Here ΔE is the difference between the strain-free equilibrium potential and the real discharge equilibrium potential. Moreover, from the crossover capacity Q_r between the two-phase and one-phase regions, one can deduce the proportion of the active materials actually involved during discharging:

$$\theta = Q_r/Q_{th} \quad (1)$$

It turns out that the θ for the nano-Li_2S – nano-LPS, nano-Li_2S – micro-LPS and micro-Li_2S – nano-LPS cathodes are 90.5%, 88.4% and 23.3%, respectively.

Figure 6(b) shows the evolution of the potential E as a function of the square root of time t during a typical titration of the nano-Li_2S – nano-LPS cathode. The linear behavior of E versus $\sqrt{t}$ indicates that the kinetics of the titration is diffusion-controlled. Therefore, the conventional GITT model is still applied for the Li_2S composite cathodes [36], except that the relationship $\mathrm{d}\delta/\mathrm{d}E$, is estimated from the one-phase regions as described above. Then the chemical diffusion coefficient of Li in Li_2S can be deduced as follow:

$$D = K_E\left(\frac{\tilde{V}}{\theta\tilde{S}}\right)^2 \quad (2)$$

$$K_E = \frac{4}{\pi}\left(\frac{I}{nF}\Big/\frac{d\delta}{dE}\frac{dE}{d\sqrt{t}}\right)^2 \quad (3)$$

where $\tilde{S}$ and $\tilde{V}$ are the average surface area and volume of a single Li_2S particle, I is the titration current density, F is the Faraday's constant, and n is the molar mass of Li_2S in the

composite cathode. Approximately assuming the Li_2S particles are spherical and the diameter is d, one obtains that

$$\tilde{V}/\tilde{S} = d/6. \quad (4)$$

The experimental parameter K_E, which reflects the reaction kinetics of the cathode, can be deduced from the GITT results using Equation 3. It also links the chemical diffusion coefficient of Li with the morphology parameter $\tilde{V}/\tilde{S}$ and the reaction ratio θ by Equation 2.

The variation of K_E versus δ for the three Li_2S composite cathodes is shown in Figure 6(c). It can be found that the K_E of the nano-Li_2S – micro-LPS cathode are very close to the nano-Li_2S – nano-LPS cathode. Assuming that the cathodes have the same particle size of Li_2S, it can be deduced that both the chemical diffusion coefficient D and the reaction ratio θ are similar for the two cathodes (Table 1). This indicates that the size difference between nano-LPS and micro-LPS has no evident effect on the reaction kinetics of the Li_2S composite cathode. Differently, the K_E of the micro-Li_2S – nano-LPS cathode is much smaller than the nano-Li_2S – nano-LPS cathode, indicating the poor reaction kinetics of the former. Assuming that the Li chemical diffusion coefficient of micro-Li_2S is similar with the nano-Li_2S at the same δ, the particle size of the micro-Li_2S which participating in the electrochemical reaction turns out to be 35.6 nm. Meanwhile, 23.3% of the micro-Li_2S is active (Table 1). Since the reaction kinetics is diffusion-controlled, a critical particle size can be defined to characterize how small the active materials are required to facilitate the reaction. The GITT analysis shows that the critical size is about 35.6 nm for discharge under 0.1 C rate at 60℃, and 23.3% of the Li_2S particles in the micro-Li_2S – nano-LPS cathode reach this critical size. This critical size can also be estimated by

$d_{crit} = 2\sqrt{D\tau}$, where the diffusion coefficient is estimated to be 10^{-16} cm^2 s^{-1} and the reaction time τ to be 10 h. This results in $d_{crit} = 38\ \mathrm{nm}$, approaching the value deduced from the GITT results. This critical size should be regarded in a statistical sense. That is, the smaller the Li_2S particles are, the more portion from the surface participates in the reaction, and averagely the particles behave like particles with the critical size which are completely active (detailed explanation can be found in the Support Information). It is worth noting that the critical size is associated with the chemical diffusion coefficient and the characteristic time (or charge-discharge rate). To operate the ASSLSBs at room temperature and higher rate, the critical size of Li_2S should be further reduced. In summary, compared with the particle size of the electrolyte, reducing the particles of Li_2S in the Li_2S @ carbon composite is more deterministic for promoting the reaction kinetics of the composite cathode.

Based on Equation 2, the chemical diffusion coefficient of Li in the nano-Li_2S – nano-LPS cathode is deduced and shown in Figure 6(d). Along with the increase of δ in $Li_{\alpha+\delta}S$, the chemical diffusion coefficient decreases evidently. The chemical diffusion coefficient of Li is determined by the ionic diffusion coefficient D_{Li^+} and the electronic diffusion coefficient D_{e^-}:

$$D = \left(\frac{1}{c_{\mathrm{Li}^+}} + \frac{1}{c_{\mathrm{e}^-}}\right) \Big/ \left(\frac{1}{D_{\mathrm{Li}^+} c_{\mathrm{Li}^+}} + \frac{1}{D_{\mathrm{e}^-} c_{\mathrm{e}^-}}\right) \qquad (5)$$

where c_{Li^+} and c_{e^-} are the concentrations of ionic and electronic carriers in Li_2S, respectively. For Li_2S, the electronic conductivity (10^{-13} S cm^{-1}) is much smaller than the ionic conductivity (10^{-9} S cm^{-1}) [37]. This indicates $D_{\mathrm{Li}^+} c_{\mathrm{Li}^+} \gg D_{\mathrm{e}^-} c_{\mathrm{e}^-}$. Consequently, the chemical diffusion coefficient of Li in Li_2S is mainly determined by the electronic diffusion coefficient:

$$D \approx \left(\frac{c_{\mathrm{e}^-}}{c_{\mathrm{Li}^+}} + 1\right) D_{\mathrm{e}^-}. \qquad (6)$$

Density functional theory calculation [38] reveals that the position of Fermi level of Li_2S changes significantly with the composition. When Li_2S is in equilibrium with S, which is a Li-poor state, the Fermi level is close to the valence band and there is a rise of the hole concentration. This enhances the chemical diffusion coefficient of Li according to Equation 6. With the increase of δ, the Fermi level moves toward the mid-gap and the concentration of the electronic carriers decreases, thus resulting in the decreasing of the chemical diffusion coefficient.

To further explore the mechanism beneath the importance of forming Li_2S @ carbon nano-composite, the lithium diffusion in Li_2S is simulated with a 2-dimensional model by FEM. Two configurations are compared. For Configuration A, the bottom margin is in contact with both LPS and carbon, and the other three margins are in contact with carbon. This models a nanocomposite of Li_2S and carbon. For Configuration B, the bottom margin is in contact with both LPS and carbon, and the other three margins are in contact with LPS. This models a nanocomposite of Li_2S and the solid electrolyte. As shown by Figure 7, after 10000 s, the lithium diffusion in Configuration A is almost completed, while only a portion from the bottom is Li-diffused in Configuration B. In Configuration B, the faster diffusion of Li^+ than electron creates a build-in electrical field, which drags back the Li^+ ions and retards their diffusion. Differently, in Configuration A, the electrons can be injected into the Li_2S particle from the other three margins in contact with carbon. They neutralize the positive charge of the fast-diffusing Li^+ ions and eliminate the build-in field near the margins, which results in fast diffusion of Li^+ ions along the margins. This point is supported by the simulation results of Configuration A at 50, 200, and 1000 s, showing a rapid increase of Li^+ concentration along the margins (Figure 7). After then, the Li diffusion continues not only from the bottom margin, but also from the other three

margins towards the center in configuration A, so that the diffusion process is greatly promoted. The FEM simulation results corroborates that the Li diffusion in Li_2S can be more effectively enhanced by forming nano-composite with conductive agent, rather than with the solid electrolyte.

The composite cathode of the ASSLSBs confronts two major challenges, that is, enhancing the reaction kinetics and accommodating the large volume change of the active material. The reaction kinetics is principally controlled by the Li diffusion in Li_2S, and is limited by the electronic diffusion as discussed above. Compositing Li_2S/S and the conductive agent at nanoscale can improve the Li diffusion in Li_2S, thus is essential for enhancing the reaction kinetics. This point is also supported by the in-situ TEM study of the lithiation process of the sulfur-carbon composites [35, 39]. On the other hand, the particle size of the solid electrolyte does not play a key role to the reaction kinetic. However, small particle size and homogenous distribution of the solid electrolyte in the Li_2S composite cathode can accommodate the strain caused by the large volume change of the active material, thus improving the cycling stability. As shown in Figure 8, for the micro-Li_2S –nano-LPS cathode, a large part of the Li_2S particles exceeds the critical size d_{crit}. These large particles exhibit poor reaction kinetics, and almost do not participate in the electrochemical process of the battery. This leads to low capacity and large overpotential. Moreover, excessive particle size of Li_2S exacerbates disruption of electronic/ionic channels by volume change. For the nano-Li_2S –micro-LPS cathode, even though the nano-Li_2S @ KB composite initially endows fast reaction kinetics, the poor contact between the LPS nanoflakes and the nano-Li_2S @ KB composite cannot afford the large volume change during the cycling, and the ionic channels will be gradually destroyed. For the nano-Li_2S

– nano-LPS cathode, not only the nano-Li_2S is embedded in the micropores of KB, but also the nano-LPS fills the mesopores of KB. This benefits both the fast Li diffusion in Li_2S and the accommodation of the volume change, so that the best battery performance is achieved amongst the three samples.

Conclusions

A liquid-phase method, without ball-milling process, is developed to synthesize Li_2S-base composite cathode of ASSLSBs. This method makes it possible to independently control the size of the active material and the solid electrolyte at nanoscale or at microscale. By comparing the electrochemical performance of the three composite cathodes, the nano-Li_2S – nano-LPS, the nano-Li_2S – micro-LPS and the micro-Li_2S – nano-LPS, it is revealed that while reducing the particle size of the cathode components is beneficial for accommodating the large volume change and improving cycling stability, compositing Li_2S with conductive agent at nanoscale, rather than with the solid electrolyte, is more essential for enhancing the reaction kinetics. The critical size of the active Li_2S particles is calculated to be 35.6 nm by a modified GITT, in a cathode operating under 0.1 C rate at 60℃. By reducing the particle size of Li_2S to 9.4 nm and that of LPS to 44 nm, a liquid-phase-synthesized composite cathode shows reversible capacity and 100% utilization of Li_2S under 0.1 C rate. This study illustrates that the size requirement of the Li_2S particles is much more stringent than that of the solid electrolyte. Compositing Li_2S/S and the conductive agent at even reduced nanoscale is the most important task for developing high-performance ASSLSBs.

Author Contributions

Bo Fan: Conceptualization, Methodology, Writing-Review & Editing **Zebo Guan**: Investigation, Writing-Original Draft **Lilin Wu**: Investigation, Validation **Shibang Zhang**: Investigation, Validation **Manlin Tan:** Resource **Zhongkuan Luo**: Resource **Xianghua Zhang**: Methodology, Writing-Review & Editing **Hongli Ma**: Writing–Review & Editing **Bai Xue**: Supervision, Conceptualization, Funding acquisition

Conflicts of interest

The authors declare that they have no known competing financial interests or personal relationships that could have appeared to influence the work reported in this paper.

Acknowledgements

The work is financially supported by the Natural Science Foundation of Guangdong Province (2021A1515011725), the Stable Support Plan for Shenzhen Higher Education Institutions (20200811211215001), the Shenzhen Science and Technology Foundation (JCYJ20210324095808023), and by the Science, Technology and Innovation Commission of Shenzhen Municipality (Grant No. CJGJZD20210408092200002). Testing Technology Center of Materials and Devices in Tsinghua Shenzhen International Graduate School was also gratefully acknowledged. The authors wish to acknowledge the assistance on TEM, HAADF, and EDS received from the Electron Microscope Center of the Shenzhen University.

Supporting Information

Additional microstructure characterization of precursors and synthesized materials, including SEM, HAADF, EDS mapping, N2 adsorption and desorption isotherms. XRD patterns of the nano-LPS and the micro-LPS. Detailed parameters deduced from GITT. Fitting parameters of the EISs. Comparison of all-solid-state lithium-sulfur batteries with Li_2S-based composite cathodes.

References

[1] S. Li, D. Leng, W. Li, L. Qie, Z. Dong, Z. Cheng, Z. Fan, Recent progress in developing Li_2S cathodes for Li–S batteries, Energy Storage Mater. 27 (2020) 279-296.

https://doi.org/10.1016/j.ensm.2020.02.010

[2] J. Yi, L. Chen, Y. Liu, H. Geng, L.Z. Fan, High capacity and superior cyclic performances of all-solid-state lithium-sulfur batteries enabled by a high-conductivity $Li_{10}SnP_2S_{12}$ solid electrolyte, ACS Appl. Mater. Inter. 11 (2019) 36774-36781.

https://doi.org/10.1021/acsami.9b12846

[3] Z. Fan, B. Ding, T. Zhang, Q. Lin, V. Malgras, J. Wang, H. Dou, X. Zhang, Y. Yamauchi, Solid/Solid interfacial architecturing of solid polymer electrolyte-based all-solid-State lithium-sulfur batteries by atomic layer deposition, Small, 15 (2019) e1903952.

https://doi.org/10.1002/smll.201903952

[4] B. Fan, Z. Guan, H. Wang, L. Wu, W. Li, S. Zhang, B. Xue, Electrochemical processes in all-solid-state Li-S batteries studied by electrochemical impedance spectroscopy, Solid State Ionics, 368 (2021) 115680.

https://doi.org/10.1016/j.ssi.2021.115680

[5] M. Wu, Y. Cui, Y. Fu, Li_2S nanocrystals confined in free-standing carbon paper for high performance lithium-sulfur batteries, ACS Appl. Mater. Inter. 7 (2015) 21479-21486.

https://doi.org/10.1021/acsami.5b06615

[6] M. Agostini, J. Hassoun, J. Liu, M. Jeong, H. Nara, T. Momma, T. Osaka, Y.K. Sun, B. Scrosati, A lithium-ion sulfur battery based on a carbon - coated lithium-sulfide cathode and an electrodeposited silicon-based anode, ACS Appl. Mater. Inter. 6 (2014) 10924-10928.

https://doi.org/10.1021/am4057166

[7] S. Nanda, A. Gupta, A. Manthiram, A lithium-sulfur cell based on reversible lithium deposition from a Li_2S cathode host onto a hostless - anode substrate, Adv. Energy Mater. 8 (2018) 1801556.

https://doi.org/10.1002/aenm.201801556

[8] Y. J. Yen, S.H. Chung, A Li_2S-based catholyte/solid-state-electrolyte composite for electrochemically stable lithium-sulfur batteries, ACS Appl. Mater. Inter. 13 (2021) 58712-58722.

https://doi.org/10.1021/acsami.1c18871

[9] T. Takeuchi, H. Kageyama, K. Nakanishi, T. Ohta, A. Sakuda, T. Sakai, H. Kobayashi, H. Sakaebe, K. Tatsumi, Z. Ogumi, Application of graphite-solid electrolyte composite anode in all-solid-state lithium secondary battery with Li_2S positive electrode, Solid State Ionics, 262 (2014) 138-142.

https://doi.org/10.1016/j.ssi.2013.09.046

[10] T. Hakari, A. Hayashi, M. Tatsumisago, Highly utilized lithium sulfide active material by enhancing conductivity in all-solid-state batteries, Chem. Lett. 44 (2015) 1664-1666.

https://doi.org/10.1246/cl.150758

[11] S. Choi, I. Yoon, W.T. Nichols, D. Shin, Carbon-coated Li_2S cathode for improving the electrochemical properties of an all-solid-state lithium-sulfur battery using Li_2S-P_2S_5 solid electrolyte, Ceram. Int., 44 (2018) 7450-7453.

https://doi.org/10.1016/j.ceramint.2018.01.104

[12] H. Jiang, Y. Han, H. Wang, Q. Guo, Y. Zhu, W. Xie, C. Zheng, K. Xie, In situ generated Li_2S-LPS composite for all-solid-state lithium-sulfur battery, Ionics, 26 (2019) 2335-2342.

https://doi.org/10.1007/s11581-019-03287-9

[13] H. Jiang, Y. Han, H. Wang, Y. Zhu, Q. Guo, H. Jiang, C. Zheng, K. Xie, Li_2S-Li_3PS_4(LPS) composite synthesized by liquid-phase shaking for all-solid-state lithium-sulfur batteries with high performance, Energy Technolo. 8 (2020) 2000023.

https://doi.org/10.1002/ente.202000023

[14] H. Yan, H. Wang, D. Wang, X. Li, Z. Gong, Y. Yang, In situ generated Li_2S-C nanocomposite for high-capacity and long-life all-solid-state lithium sulfur batteries with ultrahigh areal mass loading, Nano Lett. 19 (2019) 3280-3287.

https://doi.org/10.1021/acs.nanolett.9b00882

[15] H. El-Shinawi, E.J. Cussen, S.A. Corr, A facile synthetic approach to nanostructured Li_2S cathodes for rechargeable solid-state Li-S batteries, Nanoscale, 11 (2019) 19297-19300.

https://doi.org/ 10.1039/c9nr06239d

[16] M. Jiang, G. Liu, Q. Zhang, D. Zhou, X. Yao, Ultrasmall Li_2S-carbon nanotube nanocomposites for high-rate all-solid-state lithium-sulfur batteries, ACS Appl. Mater. Inter. 13 (2021) 18666-18672.

https://doi.org/10.1021/acsami.1c00511

[17] Y. Zhu, C. Wang, Galvanostatic intermittent titration technique for phase-transformation electrodes, J. Phys. Chem. C, 114 (2010) 2830-2841.

https://doi.org/10.1021/jp9113333

[18] Y.-H. Xu, W.-Z. Li, B. Fan, P. Fan, Z.-K. Luo, F. Wang, X.-H. Zhang, H.-L. Ma, B. Xue, Stabilizing electrode/electrolyte interface in Li-S batteries using liquid/solid Li_2S-P_2S_5 hybrid electrolyte, Appl. Surf. Sci., 546 (2021).

https://doi.org/10.1016/j.apsusc.2021.149034

[19] M. Nagao, A. Hayashi, M. Tatsumisago, Sulfur–carbon composite electrode for all-solid-state Li/S battery with Li_2S–P_2S_5 solid electrolyte, Electrochim. Acta, 56 (2011) 6055-6059.

https://doi.org/10.1016/j.electacta.2011.04.084

[20] H. Wang, L. Wu, B. Xue, F. Wang, Z. Luo, X. Zhang, L. Calvez, P. Fan, B. Fan, Improving cycling stability of the lithium anode by a spin-coated high-purity Li_3PS_4 artificial SEI layer, ACS Appl. Mater. Inter. 14 (2022) 15214-15224.

https://doi.org/10.1021/acsami.1c25224

[21] L. Wu, B. Xue, H. Wang, Z. Su, Z. Luo, F. Wang, X. Zhang, L. Calvez, B. Fan, Self-densified ultrathin solid electrolyte membrane fabricated from monodispersed sulfide electrolyte nanoparticles, J. Am. Ceram. Soc. 105(12) (2022) 7344-7354.

[22] H. Wang, Z.D. Hood, Y. Xia, C. Liang, Fabrication of ultrathin solid electrolyte membranes of β-Li_3PS_4 nanoflakes by evaporation-induced self-assembly for all-solid-state batteries, J. Mater. Chem. A, 4 (2016) 8091-8096.

https://doi.org/10.1039/c6ta02294d

[23] Z. Wang, Y. Jiang, J. Wu, Y. Jiang, S. Huang, B. Zhao, Z. Chen, J. Zhang, Reaction mechanism of Li_2S-P_2S_5 system in acetonitrile based on wet chemical synthesis of $Li_7P_3S_{11}$ solid electrolyte, Chem. Eng. J. 393 (2020) 124706.

https://doi.org/10.1016/j.cej.2020.124706

[24] H. Jiang, Y. Han, H. Wang, Y. Zhu, Q. Guo, H. Jiang, C. Zheng, K. Xie, Facile synthesis of a mixed-conductive Li_2S composites for all-solid-state lithium-sulfur batteries, Ionics, 26 (2020) 4257-4265.

https://doi.org/10.1007/s11581-020-03591-9

[25] D. Wang, Y. Wu, X. Zheng, S. Tang, Z. Gong, Y. Yang, Li_2S@NC composite enable high active material loading and high Li_2S utilization for all-solid-state lithium sulfur batteries, J. Power Sources, 479 (2020) 228792.

https://doi.org/10.1016/j.jpowsour.2020.228792

[26] H. Li, T. Zhang, Z. Yang, Y. Shi, Q. Zhuang1, Y. Cui, Electrochemical impedance spectroscopy study on using $Li_{10}GeP_2S_{12}$ electrolyte for all-solid-state lithium batteries, Int. J. Electrochem. Sci. 16 (2021) 210229.

https://doi.org/10.20964/2021.02.33

[27] X. Yao, N. Huang, F. Han, Q. Zhang, H. Wan, J.P. Mwizerwa, C. Wang, X. Xu, High-performance all-solid-state lithium-sulfur batteries enabled by amorphous sulfur-coated reduced graphene oxide cathodes, Adv. Energy Mater., 7 (2017) 1602923.

https://doi.org/10.1002/aenm.201602923

[28] Q. Zhang, H. Wan, G. Liu, Z. Ding, J.P. Mwizerwa, X. Yao, Rational design of multi-channel continuous electronic/ionic conductive networks for room temperature vanadium tetrasulfide-based all-solid-state lithium-sulfur batteries, Nano Energy, 57 (2019) 771-782.

https://doi.org/10.1016/j.nanoen.2019.01.004

[29] S. Ohno, R. Koerver, G. Dewald, C. Rosenbach, P. Titscher, D. Steckermeier, A. Kwade, J. Janek, W.G. Zeier, Observation of chemomechanical failure and the influence of cutoff potentials in all-solid-state Li–S batteries, Chem. Mater. 31 (2019) 2930-2940.

https://doi.org/10.1021/acs.chemmater.9b00282

[30] A. Sakuda, H. Kitaura, A. Hayashi, K. Tadanaga, M. Tatsumisago, Modification of interface between $LiCoO_2$ electrode and Li_2S-P_2S_5 solid electrolyte using Li_2O-SiO_2 glassy layers, J. Electrochem. Soc. 156 (2009) A27-A32.

https://doi.org/10.1149/1.3005972

[31] K. Suzuki, N. Mashimo, Y. Ikeda, T. Yokoi, M. Hirayama, R. Kanno, High cycle capability of all-solid-state lithium–sulfur batteries using composite electrodes by liquid-phase and mechanical mixing, ACS Appl. Energy Mater. 1 (2018) 2373-2377.

https://doi.org/10.1021/acsaem.8b00227

[32] D.H. Kim, D.Y. Oh, K.H. Park, Y.E. Choi, Y.J. Nam, H.A. Lee, S.-M. Lee, Y.S. Jung, Infiltration of solution-processable solid electrolytes into conventional Li-ion-battery electrodes for all-solid-state Li-ion batteries, Nano Lett. 17 (2017) 3013-3020.

https://doi.org/10.1021/acs.nanolett.7b00330

[33] K.H. Park, D.Y. Oh, Y.E. Choi, Y.J. Nam, L. Han, J.-Y. Kim, H. Xin, F. Lin, S.M. Oh, Y.S. Jung, Solution-processable glass LiI-Li_4SnS_4 superionic conductors for all-solid-state Li-ion batteries, Adv. Mater. 28 (2016) 1874-1883.

https://doi.org/10.1002/adma.201505008

[34] A. Van der Ven, J. Bhattacharya, A.A. Belak, Understanding Li diffusion in Li-intercalation compounds, Acc. Chem. Res. 46 (2013) 1216-1225.

https://doi.org/10.1021/ar200329r

[35] H. Kim, J.T. Lee, A. Magasinski, K. Zhao, Y. Liu, G. Yushin, In situ TEM observation of electrochemical lithiation of sulfur confined within Inner cylindrical pores of carbon nanotubes, Adv. Energy Mater., 5 (2015) 1501306.

https://doi.org/10.1002/aenm.201501306

[36] W. Weppner, R.A. Huggins, Determination of the kinetic parameters of mixed-conducting electrodes and application to the system Li_3Sb, J. Electrochem. Soc. 124 (1977) 1569-1578.

[37] F. Han, J. Yue, X. Fan, T. Gao, C. Luo, Z. Ma, L. Suo, C. Wang, High-performance all-solid-state lithium-sulfur battery Enabled by a mixed-Conductive Li_2S nanocomposite, Nano Lett. 16 (2016) 4521-4527.

https://doi.org/10.1021/acs.nanolett.6b01754

[38] A. Moradabadi, P. Kaghazchi, Thermodynamics and kinetics of defects in Li_2S, Appl. Phys. Lett. 108 (2016) 213906.

https://doi.org/10.1063/1.4952434

[39] Z. Yang, Z. Zhu, J. Ma, D. Xiao, X. Kui, Y. Yao, R. Yu, X. Wei, L. Gu, Y.-S. Hu, H. Li, X. Zhang, Phase separation of Li_2S/S at nanoscale during electrochemical lithiation of the solid-state lithium-sulfur battery using in situ TEM, Adv. Energy Mater. 6 (2016) 1600806.

https://doi.org/10.1002/aenm.201600806

Tables

Table 1. Chemical diffusion coefficient D, Li_2S particle size d and reaction ratio θ of the three composite cathodes deduced from the GITT titration at δ = 0.0216.

cathodes	D (10^{-17} cm^2 s^{-1})	d (nm)	θ
nano-Li_2S – nano-LPS	4.41	9.4	90.5%
nano-Li_2S – micro-LPS	1.89	9.4	88.4%
micro-Li_2S – nano-LPS	4.41	35.6	23.3%

Figure Captions

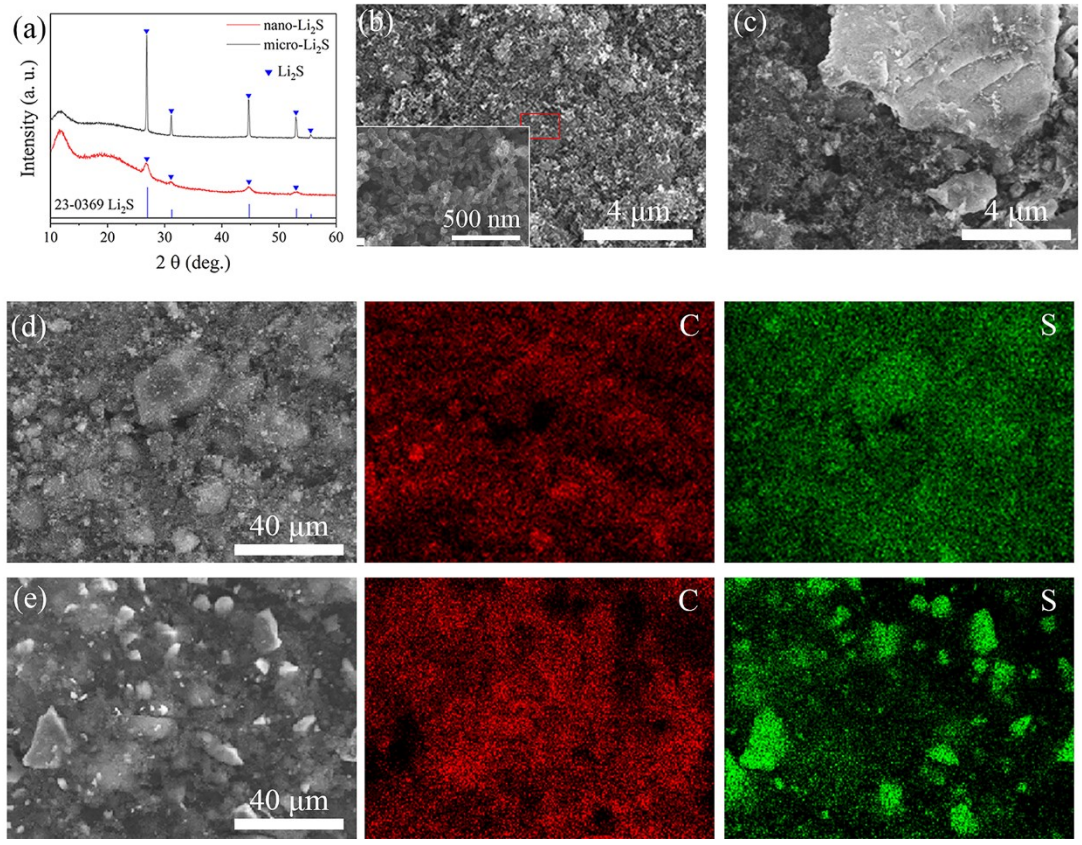

Figure 1. Characterization of the nano-Li_2S @ KB and micro-Li_2S @ KB composites. (a) XRD patterns of the two composites. High magnification SEM images of (b) the nano-Li_2S @ KB composite and (c) the micro-Li_2S @ KB composite. EDS mapping of (d) the nano-Li_2S @ KB composite and (e) the micro-Li_2S @ KB composite.

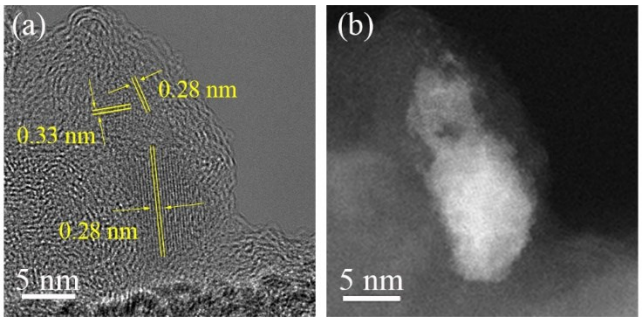

Figure 2. (a) HRTEM image of the nano-Li_2S @ KB shows that ~ 10 nm particle of Li_2S wrapped by KB. (b) High magnification HAADF image of the nano-Li_2S @ KB.

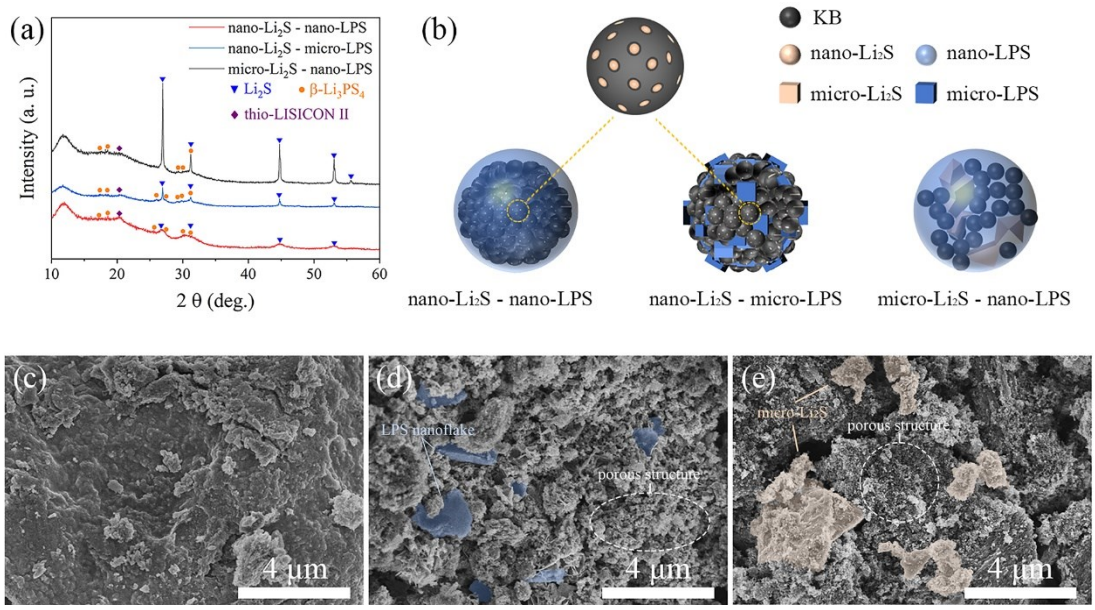

Figure 3. Characterization of the Li_2S composite cathodes. (a) XRD patterns of the three cathodes. (b) Schematic diagram describing the microstructure of the cathodes. SEM images

of (c) the nano-Li_2S – nano-LPS cathode, (d) the nano-Li_2S – micro-LPS cathode and (e) the micro-Li_2S – nano LPS cathode.

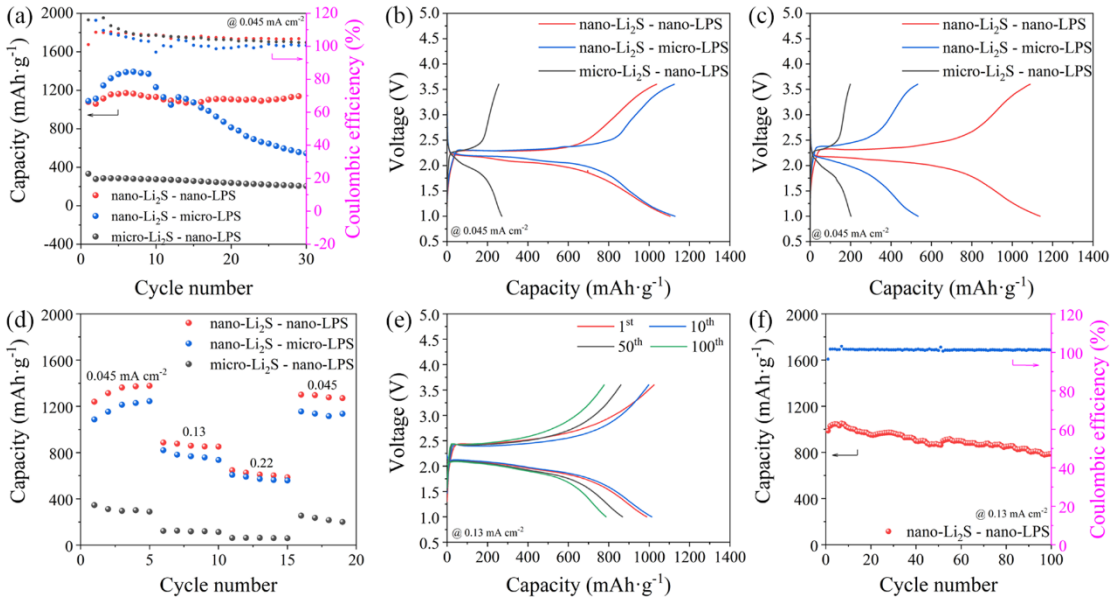

Figure 4. Battery performance with the three composite cathodes. (a) Cycling performance, charge and discharge curves of (b) the 10th cycle and (c) the 30th cycle at 0.045 mA cm^{-2}. (d) Rate performance. (e) Charge and discharge curves and (f) cycling performance with the nano-Li_2S – nano-LPS cathode at 0.13 mA cm^{-2}.

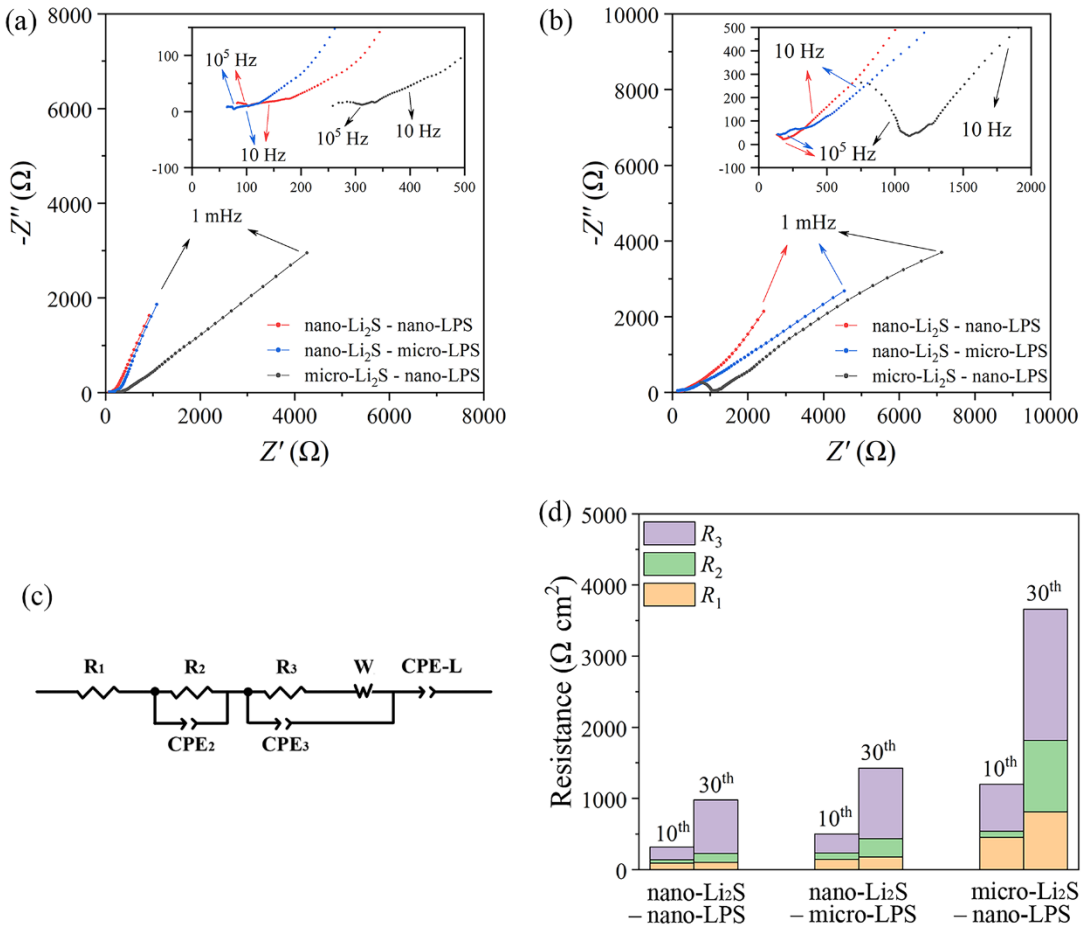

Figure 5. EIS analysis of batteries with the three composite cathodes. Nyquist plots of the batteries at (a) the 10th cycle and (b) the 30th cycle. (c) Equivalent circuit for the batteries. (d) Ohmic resistance R_1, interfacial resistance R_2 and charge transfer resistance R_3 deduced from the EISs.

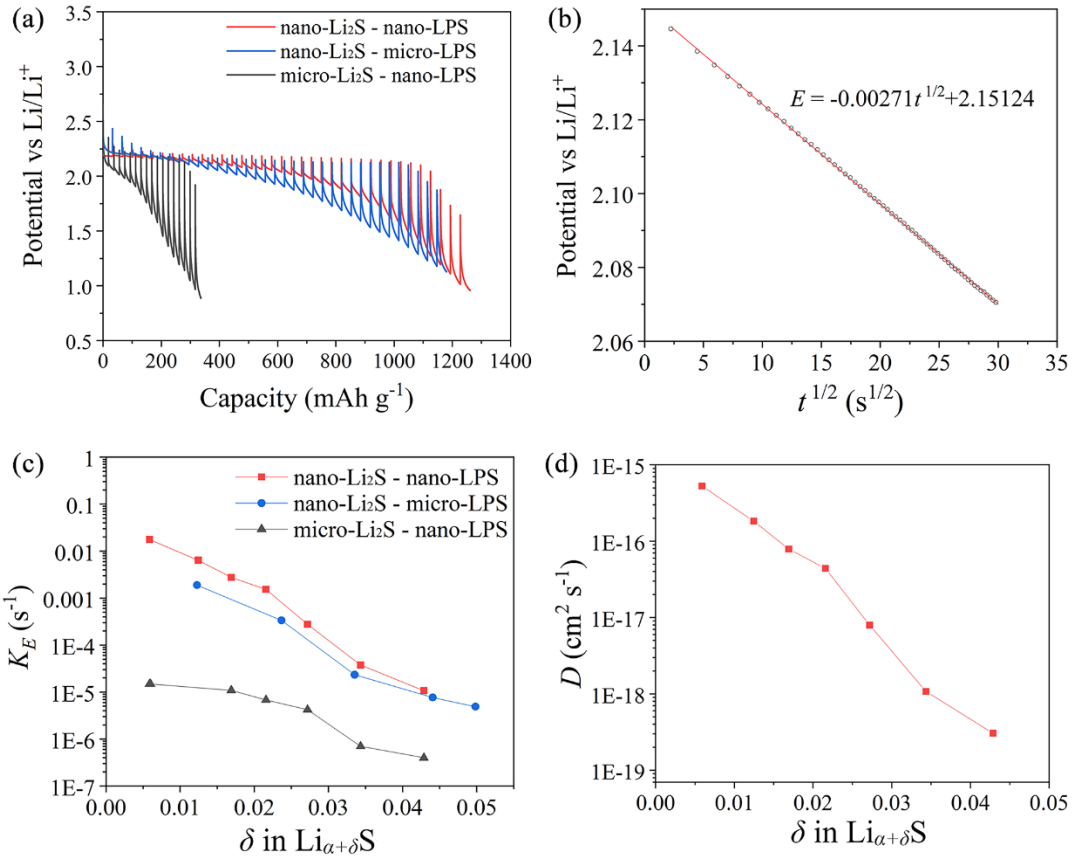

Figure 6. GITT analysis on the kinetics of the Li_2S composite cathodes. (a) GITT curves. (b) Linear behavior of E vs.$\sqrt{t}$ relationship for a single titration. (c) K_E and (d) chemical diffusion coefficient of Li vs. δ in $Li_{\delta+a}S$.

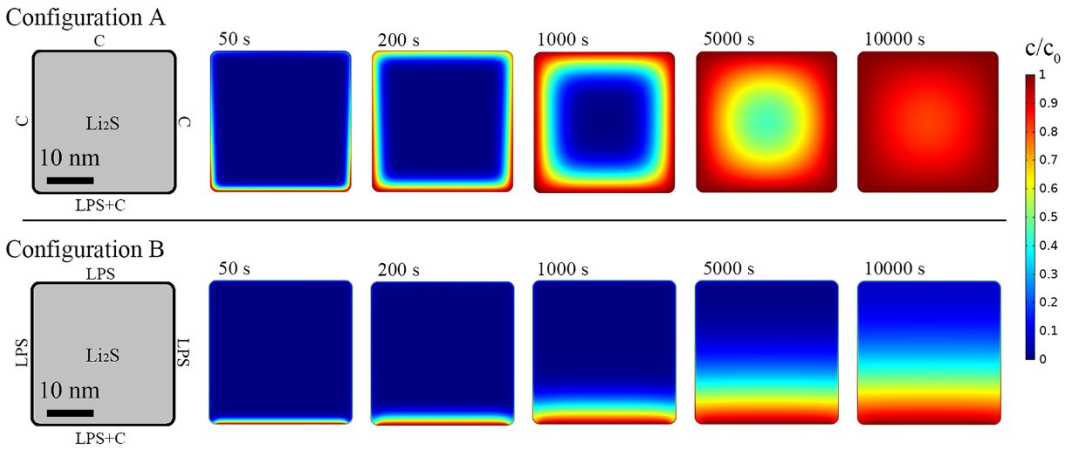

Figure 7. Simulated results of the Li diffusion in the Li_2S nanoparticle with side length of 30 nm. The color bar represents the normalized Li^+ concentration c/c_0. Since the Li diffusion is the result of the synergistic effect of Li^+ transport and electronic transport, the poorer electronic transport limits the Li diffusion, especially in Configuration B.

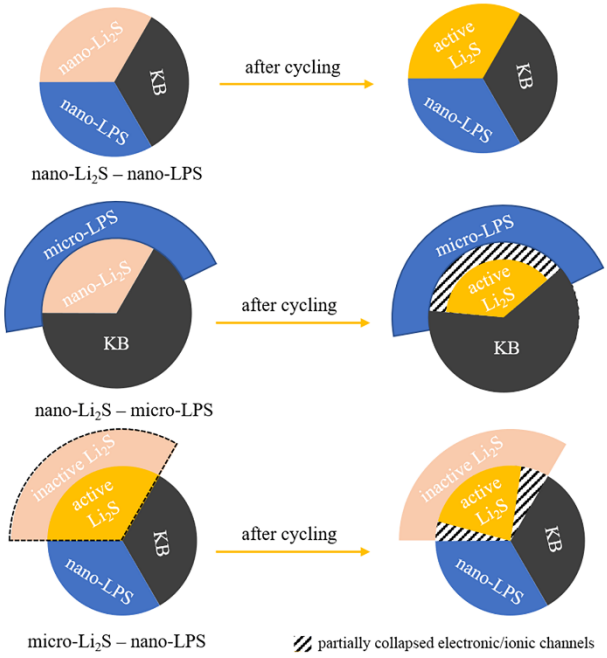

Figure 8. Schematic diagram describing the microstructure and fading mechanism of the three Li_2S composite cathodes.